



LAWRENCE
LIVERMORE
NATIONAL
LABORATORY

TEMPEST Simulations of Collisionless Damping of Geodesic-Acoustic Mode in Edge Plasma Pedestal

X. Q. Xu, Z. Xiong, W. M. Nevins, G. R. McKee

May 30, 2007

Physical Review Letters

Disclaimer

This document was prepared as an account of work sponsored by an agency of the United States Government. Neither the United States Government nor the University of California nor any of their employees, makes any warranty, express or implied, or assumes any legal liability or responsibility for the accuracy, completeness, or usefulness of any information, apparatus, product, or process disclosed, or represents that its use would not infringe privately owned rights. Reference herein to any specific commercial product, process, or service by trade name, trademark, manufacturer, or otherwise, does not necessarily constitute or imply its endorsement, recommendation, or favoring by the United States Government or the University of California. The views and opinions of authors expressed herein do not necessarily state or reflect those of the United States Government or the University of California, and shall not be used for advertising or product endorsement purposes.

TEMPEST simulations of collisionless damping of geodesic-acoustic mode in edge plasma pedestal

X. Q. Xu[†], Z. Xiong[†], W. M. Nevins[†], and G. R. McKee[‡]

[†]*Lawrence Livermore National Laboratory, Livermore, CA 94550 USA*

[‡]*University of Wisconsin-Madison, 1500 Engineering Drive, Madison, Wisconsin 53706, USA*

(Dated: May 29, 2007)

The fully nonlinear (full-f) 4D TEMPEST gyrokinetic continuum code produces frequency, collisionless damping of GAM and zonal flow with fully nonlinear Boltzmann electrons for the inverse aspect ratio ϵ -scan and the tokamak safety factor q -scan in homogeneous plasmas. The TEMPEST simulation shows that GAM exists in edge plasma pedestal for steep density and temperature gradients, and an initial GAM relaxes to the standard neoclassical residual, rather than Rosenbluth-Hinton residual due to the presence of ion-ion collisions. The enhanced GAM damping explains experimental BES measurements on the edge q scaling of the GAM amplitude.

PACS numbers: 52.55.Fa, 52.25.Fi, 52.35.Ra, 52.65.Tt

The Geodesic-Acoustic Mode (GAM) is a poloidally asymmetric mode with a coherent and radially localized poloidal flow oscillation that is dominant in the outer regions of the magnetically confined toroidal plasmas [1,2]. This mode is characterized by oscillations of the plasma column in the vertical direction with a characteristic frequency $\omega_G \geq v_{Ti}/R_0$, where R_0 is the major radius of a torus and $v_{Ti} = \sqrt{2T_i/M_i}$ the ion thermal velocity. The GAM has been clearly identified experimentally in tokamak and stellarator plasmas [3,4]. GAMs and zonal flows are driven by the turbulence, damped by collisionless Landau wave-particle resonances and by the collisional friction between trapped and circulating ions [5]. The turbulence fluctuation levels and transport are in turn regulated by the GAM and zonal flows via the time-varying $E \times B$ flow shear de-correlation [6]. This letter will focus on the new GAM damping mechanism induced by the finite-orbit-width (FOW) effect, its parametric dependence, and its relevance to the experiments.

The GAM is a normal mode, involving particle parallel ion dynamics, cross-field drifts, and acceleration. Earlier GAM theory and simulations focused on the large aspect ratio and small orbit regime. Recently the damping rate is found to be sensitive to $k_{\perp}\rho_i$ at large q [7,8], where ρ_i is the ion gyro-radius and q is the tokamak safety factor. An enhanced damping is induced by promoting the second resonant condition $v_{\parallel} = qR\omega_G/2$ due to the FOW effect of passing particles $\delta_i \sim \rho_i q$. In fact, as $k_{\psi}\delta_i$ increases, a series of resonance at $v_{\parallel} = qR\omega_G/n$ becomes effective [8]. When the resonance velocity is reduced, more passing particles participate in the resonance due to the shape of Maxwellian distribution, thus the damping is enhanced. The enhanced damping explains experimental measurements on the scaling of the GAM amplitude with edge safety factor, q_{95} [9].

We report on application of TEMPEST, a fully nonlinear (full-f) initial-value gyrokinetic code, to simulate the GAM relaxation in edge plasmas. This 5-dimensional $(\psi, \theta, \zeta, E_0, \mu)$ continuum code represents velocity space via a grid in equilibrium energy (E_0) and magnetic moment (μ) variables, and configuration space via a grid

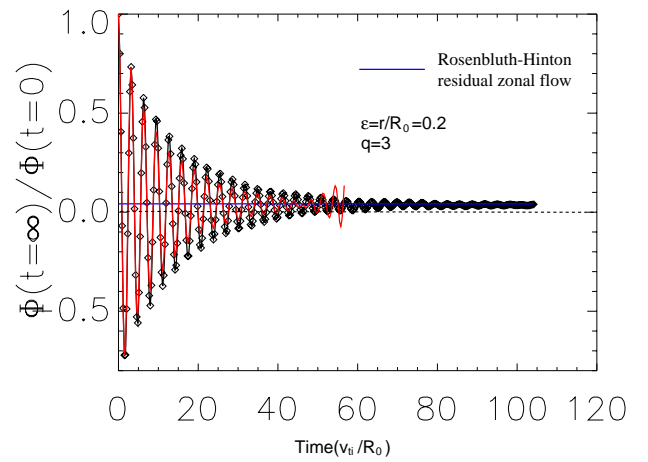


FIG. 1: Time evolution of the zonal-GAM potential shows GAM oscillation, collisionless damping, and zonal flow residual for a circular geometry with $q = 3$ and $\epsilon = 0.2$ with two different poloidal resolutions. Red solid line: $n_{\psi} = 32$, $n_{\theta} = 16$, $n_{E0} = 30$, and $n_{\mu} = 60$; Black line: $n_{\psi} = 32$, $n_{\theta} = 64$, $n_{E0} = 50$, and $n_{\mu} = 100$.

in poloidal magnetic flux (ψ), poloidal angle (θ) and toroidal angle (ζ). The geometry can be circular annulus or that of a diverted tokamak and so includes boundary conditions for both closed magnetic flux surfaces and open field lines. The same set of gyrokinetic equations are discretized for both geometries. The equations are solved via a Method-of-Lines approach and an implicit backward-differencing scheme using a Newton-Krylov iteration to advance the system in time. The spatial derivatives are discretized with finite differences while a high-order finite volume method is used in velocity space (E_0, μ). A fourth-order upwinding algorithm is used for parallel streaming, and a fifth-order WENO scheme is used for particle cross-field drifts. Boundary conditions at conducting material surfaces are implemented on the plasma side of the sheath. The code includes fully nonlinear kinetic or Boltzmann electrons. The gyrokinetic Poisson equation in the long wavelength limit $\rho_i/L_{\psi} \ll 1$ is

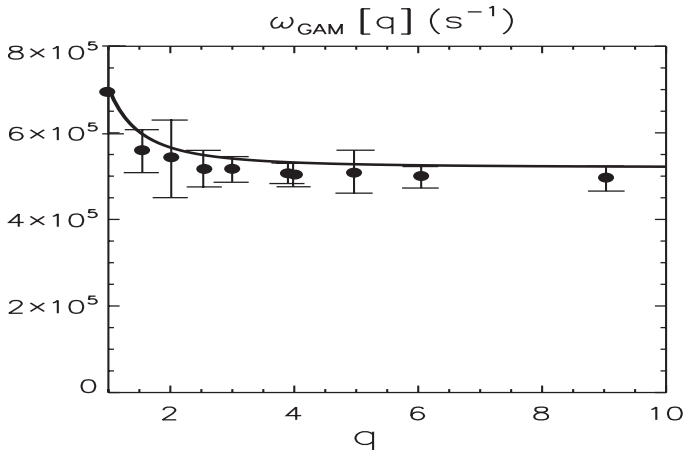


FIG. 2: GAM frequency ω_G vs q for $\epsilon = 0.2$. The black solid curve comes from theory [7] and the points are TEMPEST simulation results. The error bar covers a full width at half maximum of a spectral peak.

solved self-consistently with the gyrokinetic equations as a differential-algebraic system involving a nonlinear system solve via Newton-Krylov iteration using a multigrid preconditioned conjugate gradient (PCG) solver for the Poisson equation. Here L_ψ is the radial box size. The description of the TEMPEST equations, numerical scheme, and verification tests have been given in Ref. [10].

In our 4D TEMPEST GAM simulations for a homogeneous plasma, the initial ion distribution is a local Maxwellian. The charge is radially separated by an initial sinusoidal perturbation of the ion density with no variation within the flux surfaces $\delta n_i = \delta n_0 \sin(2\pi r/L_\psi)$. The electron model is fully nonlinear Boltzmann $n_e = \langle n_i(\psi, \theta, t = 0) \rangle \exp(e\phi/T_e) / \langle \exp(e\phi/T_e) \rangle$, where $\langle \rangle$ represents the flux surface average. This choice of coefficient for Boltzmann electron model means that there is no cross field electron transport. Both radial and poloidal boundary conditions are periodic. We consider a simple axisymmetric tokamak with the magnetic field in a circular geometry, given by $\mathbf{B} = B_\zeta \mathbf{e}_\zeta + B_\theta \mathbf{e}_\theta$, where ζ and θ are the toroidal and poloidal angles of a torus, respectively. The poloidal angle θ is chosen such that $\theta = 0$ corresponds to the outboard midplane of the torus. The inverse aspect ratio $\epsilon = r/R_0$ is not assumed to be small, where r is the minor radius. The major radius is given by $R = R_0(1 + \epsilon \cos \theta)$ and toroidal magnetic field $B_\zeta = B_0 R_0/R$. The equilibrium parameters used are toroidal magnetic field $B_0 = 15\text{T}$, major radius $R_0 = 1.71\text{m}$, and temperature $T_i = T_e = 3\text{keV}$ with deuterium ions. The magnetic field $B_\zeta(r)$ is radially uniform in the simulation domain to facilitate the radial periodic boundary conditions. The typical resolution is $n_\psi = 32, n_\theta = 64, n_{E0} = 30$ and $n_\mu = 60$.

The full-f, self-consistent TEMPEST simulation results for collisionless damping of geodesic acoustic modes and zonal flow are shown in Fig. 1 for $q = \epsilon B_0/B_\theta = 3$ and $\epsilon = 0.2$. The time unit corresponds to one GAM period

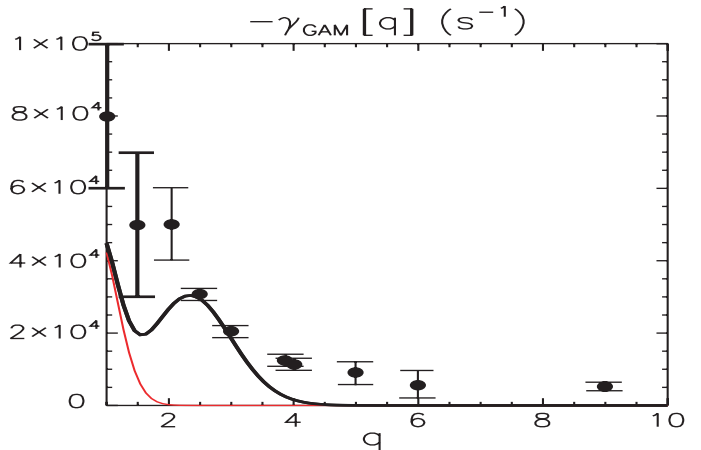


FIG. 3: GAM damping rate γ_G vs q for $\epsilon = 0.2$. The black (red) solid curve comes from theory with (without) the finite-orbit-width (FOW) effect [7] and the points are TEMPEST simulation results.

(R_0/v_{Ti}). One can see the presence of GAM oscillation, a strong collisionless Landau damping of GAM oscillation, and a nonzero undamped poloidal flow residual. The different curves corresponds to two poloidal resolutions: red solid line for $n_\psi = 32, n_\theta = 16, n_{E0} = 30$, and $n_\mu = 60$; black line for $n_\psi = 32, n_\theta = 64, n_{E0} = 50$, and $n_\mu = 100$. The high resolution run yields the same frequency, a slight improved damping rate, and eliminates the recurrence. Excellent agreement has been obtained between theory [7,8] and simulations for the GAM frequency and damping rate, and for the Rosenbluth-Hinton residual in the large aspect ratio limit.

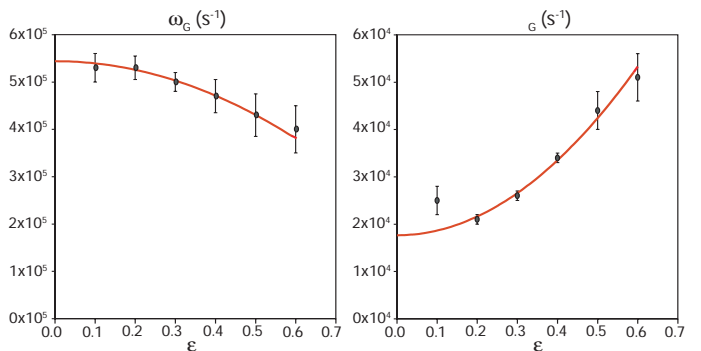


FIG. 4: GAM frequency ω_G (left) and damping rate γ_G (right) vs ϵ for $q = 3$. The black solid curve with points are TEMPEST simulation results and red solid line is a least-squares-fit to the data.

Two series of TEMPEST simulations are conducted to investigate the scaling characteristics of the GAM as a function of q and ϵ . One is a q -scan for a fixed $\epsilon = 0.2$, while other is a ϵ -scan for a fixed $q = 3$. In Fig. 2 we plot the frequency of GAM ω_G vs q for the case $\epsilon = 0.2$. The black solid curve comes from theory and the points are TEMPEST results. The error bar here and in the rest of

paper covers a full width at half maximum of a spectral peak. As one can see, excellent agreement is found between theory and simulations. The damping rate of GAM vs q is plotted in Fig. 3. The black solid curve comes from theory of Sugama and Watanabe [7] with the FOW effect. The red solid curve omits the FOW effect. The points are TEMPEST simulation results. The FOW effect dramatically enhances the GAM damping rate by inducing the multiple resonances in phase space. In general, the damping rate increases for all q as $k_\psi \rho_i$ increases. However, for a given $k_\psi \rho_i \simeq 0.14$ the enhancement is not monotonic as q increases, and especially strong in the range of $1.5 < q < 4$. For the same parameters, the damping rate is almost zero if the FOW effect is ignored. Although the simulation results are qualitatively consistent with the theory, the simulations yield a higher damping rate. The theoretical expression assumed $\epsilon \ll 1$ and $q^2 \gg 1$ expansions while retaining an additional damping at the 2nd resonance $v_{\parallel} \simeq \omega_G q R_0 / 2$ accurate for passing ions only. This may give a quantitative error when $q < 2$ since the 2nd harmonic resonance with trapped particles might further enhance the damping due to its FOW effect $\delta_{tr} \sim q \rho_i / \sqrt{\epsilon}$. A simple estimate shows that this trapped particle resonance might increase the GAM damping by as much as a factor of 2, which is consistent with our simulations. The large damping leads to a few oscillations in the time series of the TEMPEST simulation data, which yields a large error bar in spectral analysis. For large q , one would expect a close comparison between TEMPEST and theory. However, increasing resolution or the top of energy meshes just improves a little on the comparisons. Therefore this leads to a possibility that a series of resonance at higher harmonics $v_{\parallel} \simeq \omega_G q R_0 / n$ with $n > 2$ become effective since they are proportional to $R_n \propto (k_\psi \rho_i q)^n \exp(-\alpha_0 q^2 / n^2)$ when q increases, where $\alpha_0 \sim 1$. For our simulation parameters, $k_\psi \rho_i \simeq 0.14$, $R_n \rightarrow R_2$ when $q \geq 4$. These resonances exist in the TEMPEST simulations, but they are not retained in the recent theories [7,8]. The contour plots of the perturbed ion gyrocenter distribution function $\delta F = F(\psi, \theta, E_0, \mu, t) - F(\psi, \theta, E_0, \mu, t = 0)$ on the $(v_{\parallel}, v_{\perp})$ space obtained by simulations clearly show the boundary of the trapped and passing ions, and the multiple vertical stripes at the resonance velocities $v_{\parallel} \simeq \omega_G q R_0 / n$ ($n \simeq 2, 3, \dots$) in the passing region.

In Fig. 4 we plot the frequency ω_G and damping rate γ_G of GAM vs ϵ for the case $q = 3$. The points are TEMPEST results and a least-squares-fit is the red solid line. The fit is given by the following formula: $\omega - i\gamma = \omega_0 - i\gamma_0 + \alpha\epsilon^2$ with $\omega_0 = 5.44 \times 10^5/s$, $\gamma_0 = 1.77 \times 10^4/s$, $\alpha = -4.54 \times 10^5/s - i0.99 \times 10^5/s$. We can interpret ω_0 and γ_0 as an extrapolation of our finite ϵ data back to $\epsilon = 0$. Hence, we would expect them to equal the $\epsilon \rightarrow 0$ theory values: $\omega_{SW} = 5.42 \times 10^5/s$, $\gamma_{SW} = 1.85 \times 10^4/s$. As one can see, the agreement is to better than 1% for ω_G , and better than 5% for γ_G . The damping rate rises for $\epsilon = 0.1$ because the radial orbit size is greater than the radial box size, so that the radial

periodic boundary condition is no longer a good approximation. The ϵ -dependence may come from the effect of the mirror force on the passing ions, which have been omitted in the theoretical analysis.

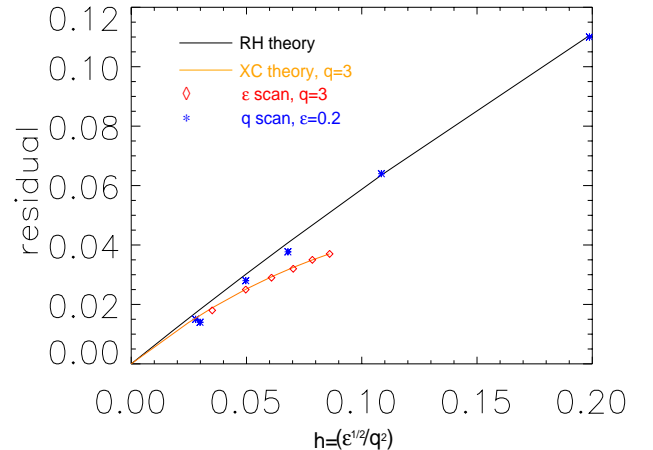


FIG. 5: Residual flux surface averaged flow fraction $\phi(t = \infty)/\phi(t = 0)$ versus Rosenbluth-Hinton parameter $h = \sqrt{\epsilon}/q^2$. The diamond points are gyrokinetic code TEMPEST results and the black curve is the prediction of Ref. [5] and the yellow curve is the prediction of Ref. [11].

Rosenbluth and Hinton's (RH) analytic calculation has shown that the linear collisionless kinetic mechanisms damp the GAM oscillation, but do not damp the zonal flows completely due to the trapped ion dynamics [5]. For the large aspect ratio, circular tokamak geometry with $k_\psi \rho_i \ll k_\psi \rho_{\theta,i} \ll 1$, the theoretical prediction for the ratio of the late time residual potential to the initial potential is given as a function $\phi(t = \infty)/\phi(t = 0) = 1/(1 + 1.6/h)$ of the single parameter $h = \sqrt{\epsilon}/q^2$. The reduction of an initial zonal flow potential is due to the neoclassical enhancement of polarization shielding. Here $\rho_{\theta,i}$ is the ion gyro-radius at the poloidal magnetic field. When explicitly evaluating plasma shaping effects on the collisionless residual zonal flow, Xiao and Catto (XC) found an expression with higher order ϵ corrections retained that act to reduce the residual zonal flow level [11]. Figure 5 shows the fractional residual potential for two scans (varying q with $\epsilon = 0.2$ and ϵ with $q = 3$, respectively) from TEMPEST simulations along with the predictions of Ref. [5,11]. An excellent agreement is observed for q scaling with RH and for ϵ -scaling with XC. The contour plots of the perturbed ion gyrocenter distribution function δF at this stage on the $(v_{\parallel}, v_{\perp})$ space obtained by simulations show fine coherent structures along the boundary of the trapped and passing ions in the trapped region (neoclassical polarization) and ballistic-mode structures along the v_{\perp} direction due to the phase mixing. A small amount ion-ion collision in a collisionality scan is found to eliminate the fine phase-space structures and therefore damp the residual zonal flows.

In an inhomogeneous plasmas with the density

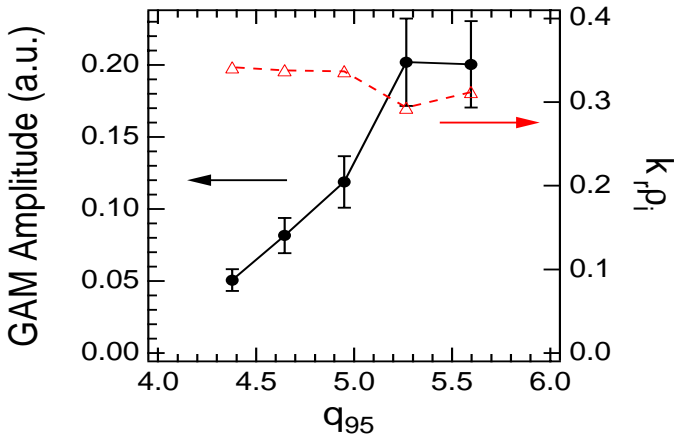


FIG. 6: Integrated GAM amplitude versus q_{95} within one discharge near $r/a = 0.9$ during the current ramp up (acquired at 100ms intervals) from Ref. [9].

and temperature profiles for the edge pedestal plasmas the simulations are carried out for large aspect ratio circular geometry with magnetic field $B_t = 7.5T$, $R_0 = 45.6m$, $q = 3$ and $\epsilon = 0.1$. The ion density and temperature profiles are initialized as a hyperbolic tangent (tanh) function of radius centered around the middle of simulation domain [$N(\psi) = n_0 + n_m \tanh((\psi - \psi_m)/\Delta_n)$], where $\psi_m = (\psi_w - \psi_c)/2$ and $\Delta_n = \delta_n \ln(N_c/N_w)$. The δ_n is a parameter to control the radial scale length. In this simulation $\delta_n = 50.5$ and a Krook collision model is used with $\nu_{ii} = 0.15v_{Ti}/R_0$. The boundary ion distribution is a fixed Maxwellian with $N_c = N(\psi_c) = 1 \times 10^{20}m^{-3}$, $N_w = N(\psi_w) = 5 \times 10^{19}m^{-3}$, $T_i(\psi_c) = 3keV$, and $T_i(\psi_w) = 1.5keV$ during a simulation. The radial boundary condition for the potential is $\partial\phi(\psi_c)/\partial\psi = \phi(\psi_w) = 0$. The electron model is the fully nonlinear Boltzmann model. The radial electric field from TEMPEST simulations agrees very well with the standard neoclassical expression $\langle U_{i\parallel} \rangle = (cT_i/Z_i e B_p) [k(\partial \ln T_i / \partial r) - (\partial \ln P_i / \partial r) - (Z_i e / T_i)(\partial \langle \Phi \rangle / \partial r)]$ with $k = -0.5$. The radial electric field is generated due to the neoclassical polarization. A time history of the flux surface averaged electric potential shows geodesic acoustic oscillations generated by the initial conditions, which then relax to a near steady state. Due to ion-ion collisions, the Rosenbluth-Hinton residual is damped, and the neoclassical residual is reached [10].

A set of experiments were performed at DIII-D to discern the scaling characteristics of the GAM as a function of the edge safety factor, q_{95} [3]. The q_{95} is a simple measure to quantify the safety factor q at the 95% flux surface for the edge plasma because the q diverges as one approaches to the magnetic separatrix. The GAM is isolated experimentally by measuring the time dependent poloidal flow of turbulence and then by applying time-delay-estimation techniques to multi-point, radially and poloidally resolved density fluctuation measurements ob-

tained with beam emission spectroscopy (BES). Fig. 6 shows that the GAM amplitude has a strong dependence on q_{95} , with the GAM increasing in amplitude between $4.2 < q_{95} < 6.0$, and undetectable at lower q_{95} . This observation is qualitatively consistent with the strong dependence on the safety factor q of the collisionless kinetic damping rate from the linear theoretical calculations and nonlinear TEMPEST simulations as shown in Fig. 3 that GAM should be strongly damped at low q_{95} due to the enhanced resonant passing ion Landau damping. The measured GAM $k_r \rho_i \simeq 0.3 - 0.35$ with little dependence on q_{95} is higher than those in our simulations $k_r \rho_i \simeq 0.14$, which would further enhance the multiple-resonance damping due to the FOW effect of passing particles $k_r \delta_i \sim k_r \rho_i q$. The qualitative consistency has also been observed between TEMPEST simulations of the RH residual in Fig. 5 and the experimental detection of zero-mean-frequency (ZMF) zonal flows that the ZMF zonal flows disappears toward the plasma edge, both due to the high q and high collisionality [12].

In conclusion, TEMPEST simulations have demonstrated an enhanced collisionless Landau damping due to the FOW effect. $k_\psi \rho_i q$. The enhancement is not monotonic as q increases, and especially strong in the range of $1.5 < q < 4$, which is qualitative consistent with BES GAM amplitude measurements. Good agreement is found between theory and simulations for systematic q -scans, ϵ -scans, and collisionality scans, and neoclassical radial electric field E_r for edge pedestal plasma, giving confidence in the TEMPEST simulations.

Acknowledgments

Authors wishing to acknowledge encouragement from Drs. J. D. Lindl and W. A. Lokke. We thank Drs. M. R. Dorr, J. A. Hittinger, and P. Colella for math-code infrastructures supports and Drs. E. Belli, J. Candy, B. I. Cohen, R. H. Cohen, G. D. Kerbel, S. Krasheninnikov, H. Qin, T. D. Rognlien, P. B. Snyder, M. V. Uman'sky, and C. X Yu for fruitful physics discussions

- [1] N. Winsor *et al.*, Phys. Fluids **11**, 2448 (1968).
- [2] K. Hallatschek *et al.*, Phys. Rev. Lett. **86**, 1223(2001).
- [3] G. R. McKee *et al.*, Phys. Plasmas **10**, 1712 (2003)
- [4] G. Conway *et al.*, IAEA-CN-149/EX/2-1.
- [5] M. N. Rosenbluth and F. L. Hinton, Phys. Rev. Lett. **80**, 724 (1998).
- [6] P. H. Diamond *et al.*, Plasma Phys. Control. Fusion **47**, R35-R161(2005).
- [7] Sugama H *et al.*, J. Phys. Plasmas **72**, 825(2006).
- [8] G. Zhe *et al.*, IAEA-CN-149/TH/P2-5.
- [9] G. R. McKee *et al.*, Plasma Phys. Control. Fusion **48**, s123(2006).
- [10] X. Q. Xu *et al.*, 2007 accepted by Nuclear Fusion.
- [11] Y. Xiao *et al.*, Phys. Plasmas **13**, 082307(2006).
- [12] D. Gupta *et al.*, Phys. Rev. Lett. **97**, 125002 (2006).

This work was performed under the auspices of the U.S. Department of Energy by University of California, Lawrence Livermore National Laboratory under Contract W-7405-Eng-48.